CHAPTER 5

Image Deconvolution in the Moment Domain

Barmak Honarvar Shakibaei and Jan Flusser

We propose a novel algorithm for image deconvolution from the geometric moments (GMs) of a degraded image by a circular or elliptical Gaussian point-spread function (PSF). In the proposed scheme, to show the invertibility of the moment equation in a closed form, we establish a relationship between the moments of the degraded image and the moments of the original image and the Gaussian PSF. The proposed inverted formula paves the way to reconstruct the original image using the Stirling numbers of the first kind. We validate the theoretical analysis of the proposed scheme and confirm its feasibility through the comparative studies.

Barmak Honarvar Shakibaei
Department of Electrical, Faculty of Engineering, University of Malaya
Lembah Pantai, 50603 Kuala Lumpur, Malaysia
e-mail: barmak.honarvar@gmail.com

Jan Flusser
Institute of Information Theory and Automation of ASCR
182 08 Prague 8, Czech Republic
e-mail: flusser@utia.cas.cz

Editor: G.A. Papakostas, *Moments and Moment Invariants - Theory and Applications*
DOI: 10.15579/gcsr.vol1.ch5, GCSR Vol. 1, ©Science Gate Publishing 2014

5.1 Introduction

In image analysis, moments are usually connected with automatic object recognition. Moment invariants, which serve as features for object description, have become an established discipline in image analysis. Among numerous descriptors used for this purpose, moments and moment invariants play a very important role and often serve as a reference state-of-the-art method for performance evaluation (interested readers can find a comprehensive survey of moment invariants in [11]).

In the long history of moment invariants, one can identify a few milestones that substantially influenced further development. The first one was in 1962, when Hu [14] employed the results of the theory of algebraic invariants, which was thoroughly studied in 19th century by Gordan and Hilbert [12], and derived his seven famous invariants to rotation of 2D objects. This was the date when moment invariants were introduced to broader pattern recognition and image processing community. The second landmark dates in 1991 when Reiss [27] and Flusser and Suk [8] independently discovered and corrected a mistake in so-called Fundamental Theorem and derived first correct sets of moment invariants to general affine transformation. The third turning point was in 1998 when Flusser and Suk [9] introduced a new class of moment-based image descriptors which are invariant to convolution of an image with an arbitrary centrosymmetric kernel, which was later extended to other specific symmetries [11]. Since that time, moment invariants have been able to handle not only geometric distortions of the images as before but also blurring and filtering in intensity domain.

Moment invariants to convolution have found numerous applications, namely in image matching and registration of satellite and aerial images [9, 24, 5, 20, 15], in medical imaging [4, 3, 32, 2], in face recognition on out-of-focus photographs [10], in normalizing blurred images into canonical forms [34, 36], in blurred digit and character recognition [21], in robot control [29], in image forgery detection [22, 23], in traffic sign recognition [19, 18], in fish shape-based classification [35], in weed recognition [26], and in cell recognition [25]. Their popularity follows from the fact that the convolution model of image formation

$$g(x,y) = (f * h)(x,y), \tag{5.1}$$

where $g(x,y)$ is the acquired blurred image of a scene $f(x,y)$ and the kernel $h(x,y)$ stands for the point-spread function (PSF) of the imaging system, is widely accepted and frequently used compromise between universality and simplicity. The model Eq.(5.1) is general enough to describe many practical situations such as out-of-focus blur of a flat scene, motion blur of a flat scene in case of translational motion, motion blur of a 3D scene caused by camera rotation around x or y axis, and media turbulence blur.

In this chapter, we demonstrate yet another application of moments when dealing with the model Eq.(5.1). If we want to invert Eq.(5.1) and actually want to estimate the original $f(x,y)$, we face an extremely ill-posed and ill-conditioned problem, even if the PSF is known. This task is known as *image deconvolution* and has been studied in hundreds of papers since the 60's. If the PSF is known, traditional techniques such as inverse filtering, Wiener filtering [1], and constrained deconvolution methods [6] can be applied. If the PSF is unknown, the task turns to so-called *blind deconvolution*

(see [17] and [7] for a basic survey) which is much more challenging and complicated. One of the possible approaches is to perform the deconvolution in a moment domain. This idea is relatively recent, it was firstly proposed in [13] and [16]. The core idea is to employ the relation between the moments of the blurred image on one side and the moments of the original and the PSF on the other side. Although this relation is known for arbitrary PSF (see [11]), its usage is efficient for PSF some moments of which are zero. In this chapter we assume the PSF is a Gaussian, either of "circular" or "elliptic" shape. We show that in this case the moment equation can be inverted by symbolic computation, i.e. the moments of the original image can be expressed as functions of the moments of the blurred image and those of the PSF in a closed form. Having this in hands, we can reconstruct the original image from its moments.

The chapter is organized as follows. In Section 5.2, we show the representation of blur model in moment domain. We derive a relationship between the original image moments and the moments of its blurred image if the PSF is a Gaussian. The image deblurring process by means of moments is shown in Section 5.3. In Section 5.4, the computational aspects of the proposed algorithm are outlined through experimental evaluation and comparison with traditional techniques. Finally, Section 5.5 concludes the chapter.

5.2 Blur Model in the Geometric Moment Domain

In this Section, we show and employ the relationship between the moments of the blurred image and those of the PSF and the original. We work with geometric moments (GM) for simplicity but all the following considerations can be re-made for any kind of orthogonal (OG) moments, too. Using OG moments might bring certain advantage in numerical computation but from theoretical point of view all kinds of moments are equivalent.

An image is a real discrete 2D function of the size $N \times M$. The GM of order $(p+q)$ of an image $f(x, y)$ is defined by

$$m_{pq} = \sum_{x=1}^{N} \sum_{y=1}^{M} x^p y^q f(x, y). \tag{5.2}$$

This discrete-domain definition is just an approximation of the traditional continuous-domain definition but it is fully sufficient for our purpose.

Assuming that the image acquisition time is so short that the blurring factors do not change during the image formation and also assuming that the blurring is of the same kind for all colors/gray-levels, we modeled the observed blurred image by a convolution Eq.(5.1). Flusser and Suk [9] obtained a classical relations for the GMs of the blurred images in terms of the original image and PSF moments as

$$m_{pq}^{(g)} = \sum_{k=0}^{p} \sum_{l=0}^{q} \binom{p}{k} \binom{q}{l} m_{kl}^{(h)} m_{p-k,q-l}^{(f)}, \tag{5.3}$$

where $m_{pq}^{(g)}$, $m_{pq}^{(h)}$ and $m_{pq}^{(f)}$ are the GMs of the degraded image, PSF and the original image, respectively. Equation 5.3 is valid for any p and q.

Provided that the PSF is a Gaussian, Eq.(5.3) is substantially simplified because many moments $m_{pq}^{(h)}$ are zero and the others can be expressed analytically. We do not restrict to circularly symmetric Gaussians but we allow arbitrary anisotropic ("elliptical") Gaussians in an axial position. We denote such PSF as $h_{\sigma_1,\sigma_2}(x,y)$.

$$h_{\sigma_1,\sigma_2}(x,y) = h_{\sigma_1}(x)h_{\sigma_2}(y), \tag{5.4}$$

where $\sigma_1, \sigma_2 > 0$ and $h_{\sigma_1}(x), h_{\sigma_2}(y)$ are 1D Gaussian functions of a traditional form

$$h_{\sigma_i}(x) = \frac{1}{\sqrt{2\pi}\sigma_i} e^{-\frac{x^2}{2\sigma_i^2}}. \tag{5.5}$$

The moments of Gaussian PSF can be expressed explicitly as

$$m_{pq}^{(h_{\sigma_1,\sigma_2})} = \begin{cases} (p-1)!!(q-1)!!\sigma_1^p\sigma_2^q & \text{if both } p \text{and } q \text{are even} \\ 0 & \text{otherwise.} \end{cases} \tag{5.6}$$

where !! denotes a double factorial[1]. Substituting the non-zero values of Eq.(5.6) into Eq.(5.3) yields

$$m_{pq}^{(g)} = \sum_{\substack{k=0 \\ k=even}}^{p} \sum_{\substack{l=0 \\ l=even}}^{q} \binom{p}{k}\binom{q}{l}(k-1)!!(l-1)!!\sigma_1^k\sigma_2^l m_{p-k,q-l}^{(f)}. \tag{5.7}$$

Equation 5.7 is actually a system of linear equations with a triangular matrix of Pascal type. Such matrices used to be ill-conditioned and their numeric inversion may be unstable. Fortunately, for Gaussian blur the inversion can be done via symbolic computation which partially overcomes the problem. Doing so, we obtain an inverse relation

$$m_{pq}^{(f)} = \sum_{\substack{k=0 \\ k=even}}^{p} \sum_{\substack{l=0 \\ l=even}}^{q} \binom{p}{k}\binom{q}{l}(-1)^{\frac{k+l}{2}}(k-1)!!(l-1)!!\sigma_1^k\sigma_2^l m_{p-k,q-l}^{(g)}. \tag{5.8}$$

Note that the summations in Eq.(5.7) and Eq.(5.8) go over even indexes k and l only.

In principle, this approach can be applied to any PSF the moments of which are known but the inversion has to be done numerically, which may cause serious problems with stability.

1 $n!! = 1 \cdot 3 \cdot 5 \cdots (n-2)n$, defined for odd n only.

5.3 Image Deblurring by Means of Moments

Image deblurring is accomplished in two steps. First, the moments of the original image are computed and then the original image is reconstructed from its moments.

To perform the second step, traditional reconstruction via Fourier transform can be used. We prefer the method introduced by Honarvar *et al.* [13], who proposed a new and exact image reconstruction algorithms from a complete set of geometric moments based on the Stirling transform. Comparing with the DFT approach, their proposed method had the stability criterion when used the complete set of GMs, but the DFT method requires a large number of moment orders to create the accurate DFT coefficients. They utilized a relationship between GMs and Stirling numbers of the second kind. Then, by using the invertibility of the Stirling transform, the original image can be reconstructed from its geometric moments. They showed in the 2D case, for an $N \times M$ pixel spatial pattern $f(x,y)$, reconstruction from a complete set of GMs can be generalized as follows:

$$\begin{aligned} f(x,y) &= \sum_{p=0}^{N-1}\sum_{q=0}^{M-1}\sum_{i=0}^{N-1}\sum_{j=0}^{M-1}\frac{(-1)^{i+j-x-y}}{i!j!}\binom{i}{x}\binom{j}{y} \\ &\quad \times S_1(i+1,p+1)S_1(j+1,q+1)m_{pq}. \end{aligned} \tag{5.9}$$

where $S_1(i,p)$ is the Stirling numbers of the first kind [33].

Now, we apply the reconstruction method [13] to reconstruct the original image. Substituting Eq.(5.8) into Eq.(5.9) leads to

$$\tilde{f}_{\sigma_1,\sigma_2}(x,y)\Big|_{GM} = \sum_{p=0}^{N-1}\sum_{q=0}^{M-1}\sum_{i=0}^{N-1}\sum_{j=0}^{M-1} A_{i,j}^{p,q}(x,y) \sum_{\substack{k=0 \\ k=even}}^{p}\sum_{\substack{l=0 \\ l=even}}^{q} B_{k,l}^{p,q}(\sigma_1,\sigma_2) m_{p-k,q-l}^{(g)} \tag{5.10}$$

where

$$A_{i,j}^{p,q}(x,y) = \frac{(-1)^{i+j-x-y}}{i!j!}\binom{i}{x}\binom{j}{y} S_1(i+1,p+1)S_1(j+1,q+1), \tag{5.11}$$

and

$$B_{k,l}^{p,q}(\sigma_1,\sigma_2) = \binom{p}{k}\binom{q}{l}(-1)^{\frac{k+l}{2}}(k-1)!!(l-1)!!\sigma_1^k\sigma_2^l. \tag{5.12}$$

5.4 Experimental Studies

In this Section we illustrate the performance of the proposed approach on three kind of images - a simple computer-generated letter with an artificial blur, a real photograph with artificial blur and astronomical image with a real blur by atmospheric turbulence, see Fig.(5.1).

(a)

(b)

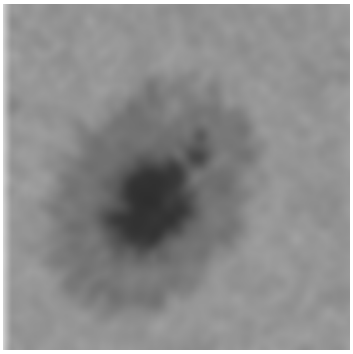

(c)

Figure 5.1: Three images used in the experiments: (a) E letter (32×32), (b) Woman (480×720), (c) Sunspot (512×512).

A limitation of our method is that in its basic version it requires a complete knowledge of the PSF, which means in case of a Gaussian the knowledge of both σ_1 and σ_2. Since this is not realistic in practice, we propose an iterative version which starts with small σ-values and converges to the true ones. Figure 5.2 shows the flowchart of the iterative version. The stop condition is based on the quality of the reconstructed image, which can be measured for instance by the statistical normalization image reconstruction error (SNIRE) [30]. SNIRE is in fact a normalized mean square error

$$\epsilon = \frac{\sum_{x=0}^{N-1} \sum_{y=0}^{M-1} \left[f(x,y) - \tilde{f}(x,y) \right]^2}{\sum_{x=0}^{N-1} \sum_{y=0}^{M-1} \left[f(x,y) \right]^2}. \tag{5.13}$$

It is suitable only in simulated experiments because it requires the knowledge of the

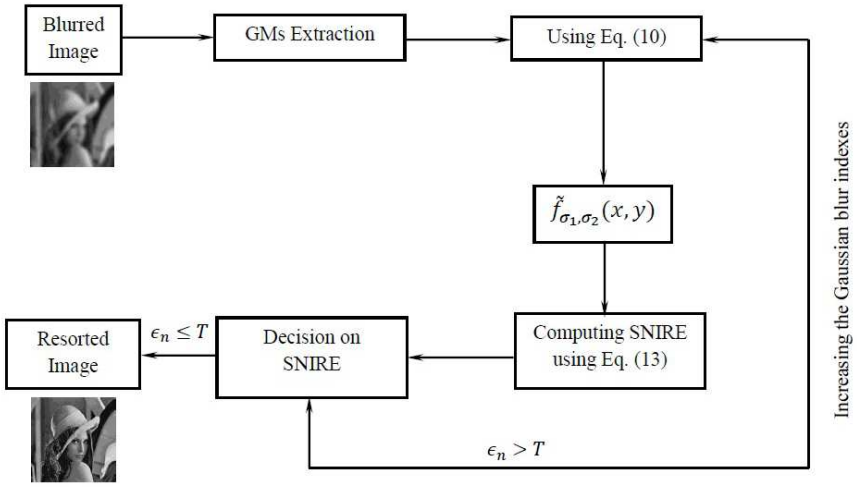

Figure 5.2: Image restoration algorithm using full set of GMs for blurred images.

ground-truth original image. Popular non-reference blur measures, such as energy of image gradient and energy contained in high-pass bands, are not suitable here because they are affected a lot by high-frequency artifacts in the restored image.

5.4.1 Simple Images Restoration

In this Subsection, we test the proposed method on the "E" letter binary image of size 32×32 as displayed in Fig.(5.1a). Since the image is small, we can use a complete set of moments without any numerical problems. As a comparative method we used standard Wiener deconvolution filter.

The first column of Table 5.1 shows the Gaussian PSFs with different values of σ_1 and σ_2 used for the blurring. The blurred images are in the second column. The third and fourth columns of this table refer to Wiener deconvolution algorithm and its error based on the subtraction of the original and restored images, $\left| f - \tilde{f} \right|$. The last column is showing the recovered images based on our algorithm using GMs' reconstruction. Below of each reconstructed image its corresponding SNIRE based on Eq.(5.13) is expressed.

In this experiment we did not use any iterations because all required parameters were known. Under these conditions, one can see that our method as well as Wiener filter yield very accurate results.

5.4.2 Deblurring of a Photograph With an Artificial Blur

In the second experiment, we used the gray-scale image, "Woman" shown in Fig. 5.1(b) of size 480×720 from LIVE database [28] as a test image. The Gaussian blur with $(\sigma_1 = \sigma_2 = 4)$ was again introduced artificially (Fig. 5.3) but this time we did not employ the knowledge of the blur parameters and we applied the iterative version

Table 5.1: Image restoration using Wiener deconvolution and proposed method for simple binary "Letter E" shown in Fig. (5.1a) with different blur kernels (below the Gaussian PSF).

Gaussian PSF (σ_1, σ_2)	Blurred image	Restored image (Wiener deconvolution)	Error $\lvert f - \tilde{f} \rvert$	Restored image (proposed method)
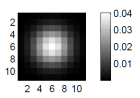	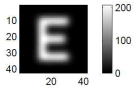	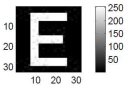	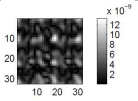	
$\sigma_1 = \sigma_2 = 2$				SNIRE=0.01156
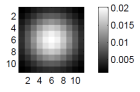	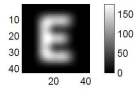	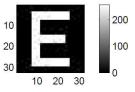	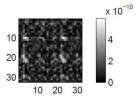	
$\sigma_1 = \sigma_2 = 3$				SNIRE=0.01983
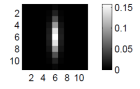	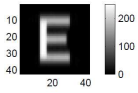	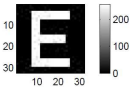	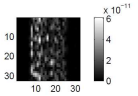	
$\sigma_1 = 0.5, \sigma_2 = 2$				SNIRE=0.02016
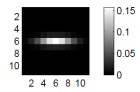	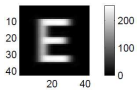		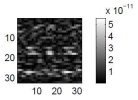	
$\sigma_1 = 2, \sigma_2 = 0.5$				SNIRE=0.02119
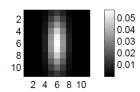	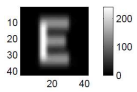		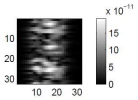	
$\sigma_1 = 1, \sigma_2 = 3$				SNIRE=0.02187
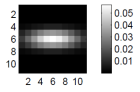	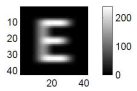		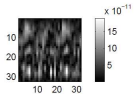	
$\sigma_1 = 3, \sigma_2 = 1$				SNIRE=0.02204

Figure 5.3: Blurred image of "Woman" using Gaussian kernel with $(\sigma_1 = \sigma_2 = 4)$.

of our algorithm and also an analogical iterative version of Wiener filter. As a quality measure we again used SNIRE.

The results are summarized in Table 5.2. The top row of Table 5.2 illustrates the results of restoration by σ going from 1 to 5 using Wiener filtering. One can observe that it yields very good result for $\sigma = 4$ but is sensitive to overestimation of σ values. Even small overestimation results in very disturbing artifacts. As one can expect, underestimation of σ leads to the result which is still slightly blurred. This is because Gaussian kernel can be expressed as a convolution of two smaller Gaussian kernels and if we restore one of them, the other one still blurs the image.

The deconvolution in moment domain yields similar results. We start iterating with a small sigma. The reconstructed image exhibits a small residual blur. Then the process converges and stops as σ approaches 4. Comparing to Wiener, both SNIRE values and visual appearance favor the moment method. The residual blur of the moment method for $\sigma = 2$ and $\sigma = 3$ is much less than that of Wiener filtering. This is the main advantage of the proposed method. On the other hand, the computational time of the moment method is significantly higher. The moment method is also more sensitive than the Wiener to overestimation of σ. If we set σ greater than the ground true value, the reconstruction collapses completely.

5.4.3 Deblurring of a Real Image

The last test which we have conducted was on real astronomical data obtained in the observation of the Sun. In the ground-based observations, the short-exposure images from the telescope are corrupted by the so-called *seeing*. This degradation leads to Gaussian-like image blurring, where the actual PSF is a composition of the intrinsic PSF of the telescope (which is constant over the observation period) and of a random component describing the perturbations of the wavefronts in the Earth atmosphere [31].

Table 5.2: Image restoration using Wiener filtering and the moment method for artificially blurred image "Woman" shown in Fig. (5.1b).

Wiener Deconvolution					
$\sigma_1 = \sigma_2 = 1$	$\sigma_1 = \sigma_2 = 2$	$\sigma_1 = \sigma_2 = 3$	$\sigma_1 = \sigma_2 = 4$	$\sigma_1 = \sigma_2 = 4.4$	$\sigma_1 = \sigma_2 = 5$
SNIRE					
0.0677	0.0675	0.0636	0.0526	0.2926	0.5766
Moment-Based Reconstruction					
				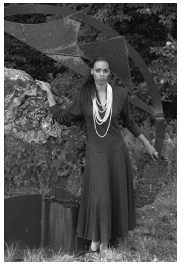	
$\sigma_1 = \sigma_2 = 0.2$	$\sigma_1 = \sigma_2 = 1$	$\sigma_1 = \sigma_2 = 2$	$\sigma_1 = \sigma_2 = 3$	$\sigma_1 = \sigma_2 = 4$	$\sigma_1 = \sigma_2 = 5$
SNIRE					
0.0609	0.0527	0.0508	0.0401	0.0170	0.5978

Table 5.3: Image reconstruction using the proposed method for "Sunspot" image shown in Fig. (5.1c) with different estimated σ (below the reconstructed images) and their corresponding SNIRE.

Blurred image	Reconstructed images				Original image
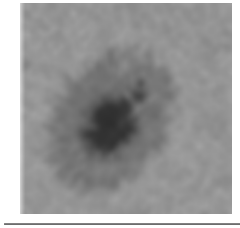	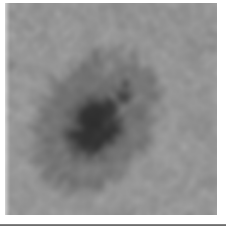	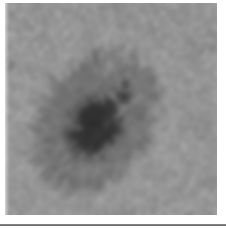	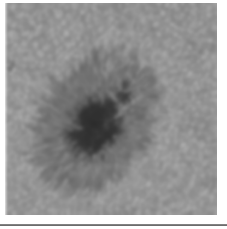	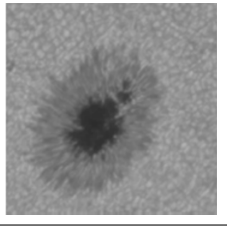	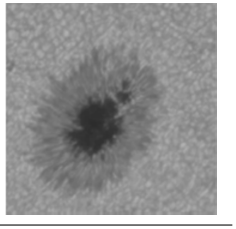
$\sigma_1 = \sigma_2$	0.2	3.2	5.7	8.6	512×512
$SNIRE$	0.2435	0.2004	0.1284	0.04257	–

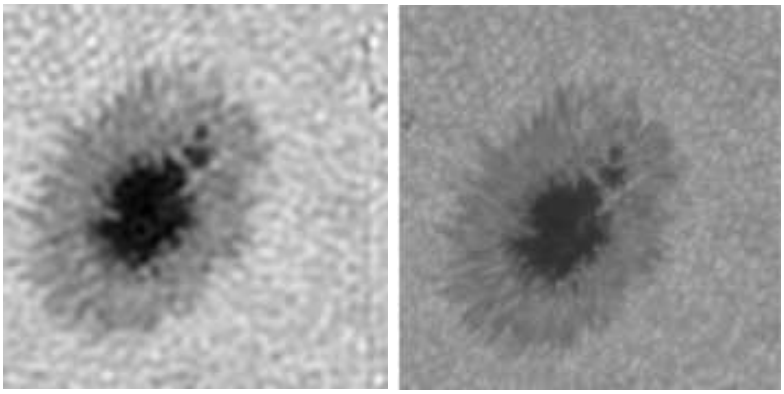

(a) (b)

Figure 5.4: Image restoration of the "Sunspot" image shown in Fig.(5.1c): (a) using Wiener filter and (b) blind deconvolution from two inputs calculated by the method from [31].

Since the seeing changes rapidly and randomly, we had several images of the same sunspot of different levels of blurring. The least blurred one we used as the "original", while the most blurred one we tried to restore. Again, the moment-based restoration was applied in an iterative manner. The SNIRE measure was calculated w.r.t. the "original". Even if this is not absolutely correct, it provides a reasonable estimation of the unknown actual SNIRE.

As can be seen from Table 5.3, the process converges reaching $\sigma = 8.6$ and yielding visually very good result with small SNIRE.

As a comparison with our method, the results of Wiener filtering and of the multichannel blind deconvolution (MBD) from two inputs calculated by the method from [31] are shown in Fig.(5.4). One can see that the moment-based method yields an output which is comparable with the "original" as well as with the result of MBD and is visually slightly better than Wiener. On the other hand, the moment method is by far the slowest.

5.5 Conclusion

In this chapter, a new approach has been proposed for image restoration from the GMs of a degraded image by a circular or elliptical Gaussian PSF. The basic step is to establish a relationship between the moments of the blurred image on one side and the moments of the original and the PSF on the other side. Although this relation is known for arbitrary PSF [11], it has not been applied for image restoration purposes.

We showed the moment equation can be inverted in a closed form and then the original image can be reconstructed using Stirling numbers of the first kind. In order to evaluate the performance of the proposed method based on image reconstruction from its GMs, simple binary image, real image which is degraded artificially and real

astronomical image have been used to test the accuracy of the proposed method. We showed that the quality of the moment method is comparable to Wiener filter and to multichannel blind deconvolution when sufficiently large number of moments is involved. Some experiments indicated that an advantage of the moment method is in its higher tolerance to underestimation of σ. A clear disadvantage however is its high computing complexity.

Acknowledgement

This work has been partially supported by the Czech Science Foundation under the Grant No. GA13-29225S.

References

[1] H.C. Andrews and B.R. Hunt. *Digital Image Restoration*. Prentice-Hall, Englewood Cliffs, NJ, 1977.

[2] Y. Bentoutou and N. Taleb. A 3-D space-time motion detection for an invariant image registration approach in digital subtraction angiography. *Computer Vision and Image Understanding*, 97(1):30–50, 2005.

[3] Y. Bentoutou and N. Taleb. Automatic extraction of control points for digital subtraction angiography image enhancement. *IEEE Transactions on Nuclear Science*, 52(1):238–246, 2005.

[4] Y. Bentoutou, N. Taleb, M. Chikr El Mezouar, M. Taleb, and J. Jetto. An invariant approach for image registration in digital subtraction angiography. *Pattern Recognition*, 35(12):2853–2865, 2002.

[5] Y. Bentoutou, N. Taleb, K. Kpalma, and J. Ronsin. An automatic image registration for applications in remote sensing. *IEEE Transactions on Geoscience and Remote Sensing*, 43(9):2127–2137, 2005.

[6] J. Biemond, R.L. Lagendijk, and R.M. Mersereau. Iterative methods for image deblurring. *Proceedings of the IEEE*, 78(5):856–883, 1990.

[7] P. Campisi and K. Egiazarian. *Blind image deconvolution: theory and applications*. CRC, 2007.

[8] J. Flusser and T. Suk. Pattern recognition by affine moment invariants. *Pattern Recognition*, 26(1):167–174, 1993.

[9] J. Flusser and T. Suk. Degraded image analysis: an invariant approach. *IEEE Transactions on Pattern Analysis and Machine Intelligence*, 20(6):590–603, 1998.

[10] J. Flusser, T. Suk, and S. Saic. Recognition of blurred images by the method of moments. *IEEE Transactions on Image Processing*, 5(3):533–538, 1996.

[11] J. Flusser, T. Suk, and B. Zitova. *Moments and Moment Invariants in Pattern Recognition*. Wiley, Chichester, United Kingdom, 2009.

[12] D. Hilbert. *Theory of Algebraic Invariants*. Cambridge University Press, Cambridge, 1993.

[13] B. Honarvar, R. Paramesran, and C.L. Lim. Image reconstruction from a complete set of geometric and complex moments. *Signal Processing*, 98:224 – 232, 2014.

[14] M.K. Hu. Visual pattern recognition by moment invariants. *IRE Transactions on Information Theory*, 8(2):179–187, 1962.

[15] S.X. Hu, Y.M. Xiong, M.Z.W. Liao, and W.F. Chen. Accurate point matching based on combined moment invariants and their new statistical metric. In *International Conference on Wavelet Analysis and Pattern Recognition (ICWAPR)*, volume 1, pages 376–381, Beijing, China, November 2007.

[16] A. Kumar, R. Paramesran, and B. Honarvar Shakibaei. Moment domain representation of nonblind image deblurring. *Applied Optics*, 53(10):B167–B171, 2014.

[17] D. Kundur and D. Hatzinakos. Blind image deconvolution. *IEEE Signal Processing Magazine*, 13(3):43–64, 1996.

[18] L. Li and G. Ma. Optimizing the performance of probabilistic neural networks using PSO in the task of traffic sign recognition. In *Advanced Intelligent Computing Theories and Applications. With Aspects of Artificial Intelligence. 4th Int. Conf. on Intelligent Computing ICIC'08*, volume 5227 of *LNCS*, pages 90–98. Springer Berlin Heidelberg, 2008.

[19] L. Li and G. Ma. Recognition of degraded traffic sign symbols using pnn and combined blur and affine invariants. In *International Conference on Natural Computation (ICNC)*, volume 3, pages 515–520. IEEE Computer Society, 2008.

[20] Z. Liu, J. An, and L. Li. A two-stage registration angorithm for oil spill aerial image by invariants-based similarity and improved ICP. *International Journal of Remote Sensing*, 32(13):3649–3664, 2011.

[21] J. Lu and Y. Yoshida. Blurred image recognition based on phase invariants. *IEICE Transactions on Fundamentals of Electronics, Communications and Computer Sciences*, E82A(8):1450–1455, 1999.

[22] B. Mahdian and S. Saic. Detection of copy-move forgery using a method based on blur moment invariants. *Forensic Science International*, 171(2-3):180–189, 2007.

[23] B. Mahdian and S. Saic. Detection of near-duplicated image regions. In *Computer Recognition Systems 2*, volume ASC 45, pages 187–195, 2007.

[24] V. Ojansivu. *Blur invariant pattern recognition and registration in the Fourier domain*. PhD thesis, University of Oulu, 2009.

[25] Z. Peng. Dynamic timber cell recognition using two-dimensional image measurement machine. *Review of Scientific Instruments*, 82(8):083703–8, 2011.

[26] Z. Peng and C. Jun. Weed recognition using image blur information. *Biosystems Engineering*, 110(2):198–205, 2011.

[27] T.H. Reiss. The revised fundamental theorem of moment invariants. *IEEE Transactions on Pattern Analysis and Machine Intelligence*, 13(8):830–834, 1991.

[28] H. Sheikh, Z. Wang, L. Cormack, and A. Bovik. Live image quality assesment database release 2. *[online]. available: http://live.ece.utexas.edu/research/quality/subjective.htm*, 2005.

[29] X.J. Shen and J.M. Pan. Monocular visual servoing based on image moments. *IEICE Transactions on Fundamentals of Electronics, Communications and Computer Sciences*, E87-A(7):1798–1803, 2004.

[30] Y. Sheng and L. Shen. Orthogonal Fourier-Mellin moments for invariant pattern recognition. *J. Opt. Soc. Am.*, 11(6):1748–1757, 1994.

[31] F. Sroubek and J. Flusser. Multichannel blind iterative image restoration. *IEEE Transactions on Image Processing*, 12(9):1094–1106, 2003.

[32] S. Tang, Y. Wang, and Y.W. Chen. Blur invariant phase correlation in X-ray digital subtraction angiography. In *International Conference on Complex Medical Engineering (ICCME)*, pages 1715–1719, 2007.

[33] N.M. Temme. *Special functions: an introduction to the classical functions of mathematical physics*. Wiley-Interscience, New York, 1996.

[34] Y. Zhang, C. Wen, and Y. Zhang. Estimation of motion parameters from blurred images. *Pattern Recognition Letters*, 21(5):425–433, 2000.

[35] Y. Zhang, C. Wen, and Y. Zhang. Neural network based classification using blur degradation and affine deformation invariant features. In *International Conference Florida Artificial Intelligence Research Society (FLAIRS)*, pages 76–80. AAAI Press, 2000.

[36] Y. Zhang, C. Wen, Y. Zhang, and Y.C. Soh. Determination of blur and affine combined invariants by normalization. *Pattern Recognition*, 35(1):211–221, 2002.